Modeling the Lateral Circulation in Straight, Stratified Estuaries*

JAMES A. LERCZAK AND W. ROCKWELL GEYER

Woods Hole Oceanographic Institution, Woods Hole, Massachussetts

(Manuscript received 6 September 2003, in final form 8 January 2004)

ABSTRACT

The dynamics of lateral circulation in an idealized, straight estuary under varying stratification conditions is investigated using a three-dimensional, hydrostatic, primitive equation model in order to determine the importance of lateral circulation to the momentum budget within the estuary. For all model runs, lateral circulation is about 4 times as strong during flood tides as during ebbs. This flood–ebb asymmetry is due to a feedback between the lateral circulation and the along-channel tidal currents, as well as to time-varying stratification over a tidal cycle. As the stratification is increased, the lateral circulation is significantly reduced because of the adverse pressure gradient set up by isopycnals being tilted by the lateral flow itself. When rotation is included, a time-dependent, cross-channel Ekman circulation is driven, and the tidally averaged, bottom lateral circulation is enhanced toward the right bank (when looking toward the ocean in the Northern Hemisphere). This asymmetry in the tidally averaged bottom lateral circulation may lead to asymmetric sediment transport, leading to asymmetric channel profiles in straight estuaries. For the weakly stratified model run, advection due to lateral currents is a dominant term in both the along-channel and cross-channel momentum equations over a tidal cycle and for the tidally averaged momentum equations. In the tidally averaged, along-channel momentum equation, lateral advection acts as a driving term for the estuarine exchange flow and can be larger than the along-channel pressure gradient. Therefore, it should not be ignored when estimating momentum budgets in estuaries.

1. Introduction

Cross-channel or lateral flows in estuaries are usually much smaller than the dominant tidal currents directed along the channel. Typically, cross-channel currents are only about 10% of the size of the along-channel tidal currents. Yet, these lateral motions can play a critical role in the dynamics of estuaries. They can set the rate at which salt and other tracers are dispersed along an estuary (Smith, 1976, 1980, 1996; West and Mangat 1986; Guymer and West 1992; Scott 1994); drive density overturns and generate intense vertical mixing (Seim and Gregg 1997); transport sediments laterally (Geyer et al. 1998; Woodruff et al. 2001); and advect along-channel momentum and, thereby, modify the along-channel momentum budget (West and Mangat 1986; Guymer and West 1992; Johnson and Ohlsen 1994; Scott 1994; Lacy and Monismith 2001; Chant 2002).

While the dynamics of lateral circulation in homogeneous (Kalkwijk and Booij 1986) and weakly stratified (Smith 1976, 1980; Nunes and Simpson 1985; Scott 1994) channels has received considerable attention, their dynamics in stratified estuaries is complex and not well understood. In this paper, we use a numerical model to explore the dynamics of lateral circulation in a straight estuarine channel with varying stratification. Our goals are to understand the importance of the lateral flow to the momentum budget within the estuary and to understand how the dynamics of the lateral flow changes with varying stratification.

Lateral flows in estuaries are driven by various mechanisms: channel curvature (Kalkwijk and Booij 1986; Geyer 1993; Seim and Gregg 1997; Chant and Wilson 1997; Chant 2002; Lacy and Monismith 2001), interactions between barotropic tidal currents and cross-channel variations in bathymetry (Li and O'Donnell 1997; Valle-Levinson et al. 2000), Coriolis forcing such as in boundary and internal Ekman layers (Johnson and Ohlsen 1994; Ott and Garrett 1998; Ott et al. 2002), cross-channel density gradients in a diffusive boundary layer over a sloping bottom (Wunsch 1970; Weatherly and Martin 1978; Garrett et al. 1993), and differential advection of along-channel density gradients (Smith 1976, 1980; Nunes and Simpson 1985; Guymer and West 1992; Scott 1994).

In this study, our model estuary is straight and the ratio of tidal amplitude to depth is small. Therefore, curvature forcing of lateral flows is not present, and

* Woods Hole Oceanographic Institution Contribution Number 10946.

Corresponding author address: James A. Lerczak, Department of Physical Oceanography, MS21, Woods Hole Oceanographic Institution, Woods Hole, MA 02543.
E-mail: jlerczak@whoi.edu

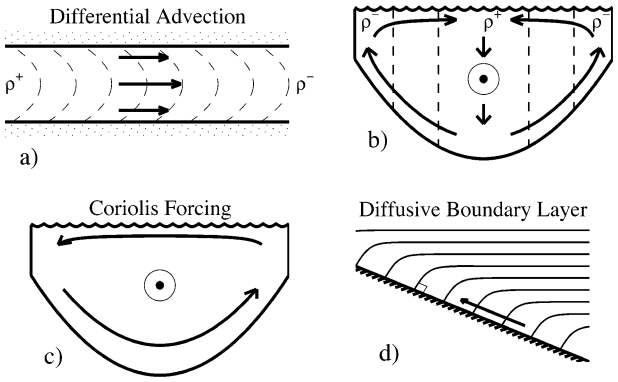

FIG. 1. (a) Schematic showing distortion of the along-channel density gradient due to differential advection during flood tide. (b) Cross-channel density gradients due to differential advection during flood tide and the lateral circulation pattern that is driven by the lateral pressure gradients. (c) Lateral circulation pattern due to Coriolis forcing during flood tide. (d) Isopycnals tilting to normal at a bottom boundary in order to satisfy a zero-buoyancy-flux boundary condition. The thick arrow indicates the direction of the circulation driven by the along-slope pressure gradient of the diffusive boundary layer.

lateral circulation driven by the interaction between the barotropic tide and bathymetric variations is negligible. Our focus, thus, is on the latter three driving mechanisms in a straight estuary: differential advection, rotation, and diffusive boundary layers.

a. Differential advection

Depth-averaged, along-channel tidal currents tend to be strongest at the deepest location of a channel cross-section (the *thalweg*) and weaker where the channel is shallow. Because of this lateral shear in the along-channel tidal currents (u_y), advection of the along-channel density gradient (ρ_x) within an estuary results in a cross-channel density gradient (ρ_y; Fig. 1a). During flood tide, for example, density is greater at the *thalweg* than at the shallower flanks. Consequently, a cross-channel baroclinic pressure gradient is set up that drives a lateral flow (Fig. 1b). Smith (1976, 1980) and Nunes and Simpson (1985) assert that the dominant balance in the lateral momentum equation is between the lateral pressure gradient and the vertical stress divergence. This is the same balance as that derived by Hansen and Rattray (1965) for the along-channel estuarine circulation. Using this balance for a vertically well mixed estuary, the lateral flow forced by differential advection scales as

$$v_{\mathrm{DA}} \sim \frac{1}{24}\frac{gH^3}{A_v B}\frac{\Delta\rho(y)}{\rho_o} \sim \frac{1}{24}\frac{gH^3}{A_v}\frac{\rho_x}{\rho_o}\frac{\Delta u(y)}{\sigma B}, \qquad (1)$$

where g is the gravitational acceleration, H is the average depth of the estuary, A_v is the vertical eddy viscosity, B is the breadth of the estuary, $\Delta\rho(y)$ is the cross-channel density difference set up by differential advection, and ρ_o is the mean density. The scale of the lateral shear in tidal currents, u_y, is expressed as $2\Delta u(y)/B$ and acts over a tidal time scale σ^{-1}, where σ is the semidiurnal tidal frequency.

By this scaling, one might expect the scale of the lateral flow to be roughly the same for flood and ebb tides since the amplitude of flood and ebb tidal currents are roughly the same and the amplitude of the lateral shear in the tidal currents might be expected to be the same during both phases of the tide. The sign of the shear would be different for flood and ebb. Therefore, the surface lateral currents would be convergent (Fig. 1b; Nunes and Simpson 1985) during floods and divergent during ebbs. However, we will show that there is a large asymmetry in the lateral circulation between flood and ebb tides. A nonlinear feedback between the lateral flow and along-channel tidal currents and time varying stratification both act to enhance the lateral flow during flood and suppress it during ebb.

b. Rotation

In a homogeneous, narrow, rotating channel the dominant balance in the cross-channel momentum equation is geostrophic with the Coriolis term nearly balancing the cross-channel barotropic pressure gradient ($fu \approx -g\zeta_y$, where ζ is the sea surface height). A lateral flow is driven by the higher-order balance between the ageostrophic along channel tidal current, cross-channel acceleration, and vertical stress divergence [see Kalkwijk and Booij (1986) for the time-independent case]. The strength of the Ekman forced lateral flow does not have a simple functional dependence on boundary layer thickness ($\beta \equiv \sqrt{2A_v/\sigma}$). However, for the range of eddy viscosities considered here ($0.1 < \beta/H < 0.4$), the strength of the lateral flow is roughly independent of β and has an amplitude of approximately

$$v_C \sim \frac{1}{8}\frac{f}{\sigma}U_o, \qquad (2)$$

where f is the Coriolis parameter and U_o is the amplitude of the along-channel tidal current (see the appendix). When the tidal boundary layer thickness is comparable to the channel depth, the flow pattern is a single circulation cell across the channel (Fig. 1c). For thin tidal boundary layers, relative to the channel depth, the structure is more complicated and varies over the tidal cycle (see the appendix).

c. Effect of stratification

Neither the differential advection nor the rotation scalings for lateral flow described above take stratification into account. In estuarine channels, the lateral flow tilts isopycnals, setting up an adverse lateral baroclinic pressure gradient that tends to suppress the lateral circulation (Seim and Gregg 1997; Chant and Wilson 1997; Chant 2002). Seim and Gregg (1997), for example, observed a dramatic difference in the ampli-

tude of the lateral flow and the resultant vertical mixing between weakly stratified and stratified conditions in a curved tidal channel in Puget Sound, Washington.

In straight, stratified estuaries without rotation, the cross-channel density gradient is caused by the differential advection of the along-channel density gradient ($\rho_x u_y$) and by the tilting of isopycnals due to the lateral flow itself ($\rho_z w_y$). Differential advection tends to accelerate the lateral flow, while tilting isopycnals tend to decelerate it. Noting that the lateral shear in vertical velocity is related to v_{DA} according to $w_y \sim HB^{-2}v_{\mathrm{DA}}$, and using (1) for the scale of v_{DA}, we obtain an expression for the relative importance of stratification in suppressing the lateral circulation:

$$\gamma \equiv \frac{\rho_z w_y}{\rho_x u_y} \sim \frac{1}{24}\frac{N^2H^2}{B^2}\frac{H^2}{A_v}\frac{1}{\sigma} = \frac{1}{24}\frac{T_{\mathrm{fr}}T_T}{T_{\mathrm{IW}}^2}, \qquad (3)$$

where N^2 is the squared buoyancy frequency ($=-g\rho_z\rho_o^{-1}$). The relative strength of these advective terms is the ratio of the frictional time scale T_{fr} and the tidal period T_T to the square of the time it takes a long internal wave to cross the channel T_{IW}. When γ is much less than 1, stratification is not important to the dynamics. However, as γ approaches 1, the pressure gradient due to isopycnal tilting becomes significant, and we predict the lateral flow will be suppressed relative to the well-mixed scaling.

d. Diffusive boundary layer

The no-flux boundary condition at the sloping channel bottom requires that the gradient of density normal to the bottom go to zero at the bottom:

$$\left.\frac{\partial\rho}{\partial n}\right|_{z=-H} = 0, \qquad (4)$$

where n is the direction normal to the bottom. As a consequence, isopycnals are tilted at the sloping boundary (Fig. 1d), resulting in a pressure gradient that drives a flow parallel to the boundary toward shallower water (Wunsch 1970; Weatherly and Martin 1978; Garrett et al. 1993). This circulation tends to destratify the fluid and acts even in the absence of differential advection and Ekman-driven lateral flows.

For a fluid with constant eddy viscosity and a Prandtl number of one (as used in this study), the steady-state circulation is confined to a boundary layer with thickness δ, given by (Garrett et al. 1993)

$$\delta^{-4} = \frac{1}{4A_v^2}(f^2 + N^2\sin^2\theta), \qquad (5)$$

where N^2 is the buoyancy frequency in the interior of the fluid, θ is the angle of the sloping bottom relative to horizontal, and f is the Coriolis frequency. The maximum strength of the alongslope circulation within the boundary layer is given by

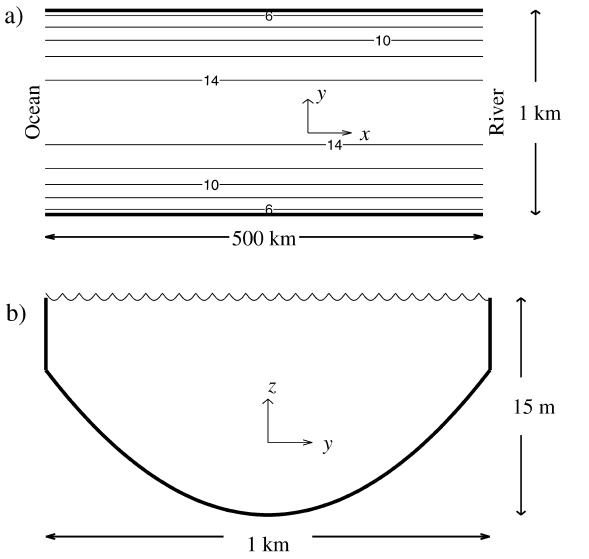

FIG. 2. Domain used in model runs. (a) Length and width of estuary with depth contoured. (b) Cross-sectional profile of estuary.

$$v_{\mathrm{BL}} \approx \frac{\sqrt{2}}{2}\frac{A_v}{\delta}\cot\theta. \qquad (6)$$

While the effect of the diffusive boundary layer will be apparent in the structure of the stratification above the bottom boundary of our model runs, we will show that the strength of the lateral circulation associated with this driving mechanism is not significant in comparison with the circulation due to differential advection and Ekman forcing. We include it here for the sake of completeness.

2. Numerical model

We model the full extent of an estuary from the ocean boundary, upriver to beyond the influence of the salinity intrusion, using the Regional Ocean Model System (ROMS; Haidvogel et al. 2000), a free-surface, hydrostatic, primitive equation model that uses a stretched, terrain-following coordinate in the vertical direction. The model domain (Fig. 2) is 500 km long and 1 km wide. The channel is straight, and the bottom has a parabolic shape with a maximum depth of 15 m in the center and a minimum depth of 5 m at the sides.

The model is forced by a barotropic tide and a time-independent downriver freshwater flux. This is accomplished by imposing, at the oceanward open boundary, a tidal flux that oscillates at the M_2 frequency and a constant downriver freshwater flux. At the landward open boundary, a radiation condition is imposed to allow the barotropic tide to radiate out of the domain and the freshwater flux to enter. The resulting tide is progressive in the upriver direction with a current amplitude of 70 cm s^{-1} and a sea-surface amplitude of 75 cm. The freshwater flux is varied in order to vary the stratification (see below).

TABLE 1. Model run parameters: A_v is the vertical eddy viscosity and diffusivity, U_f is the down-estuary freshwater velocity, $\Delta S(z)$ is the top-to-bottom salinity difference, U_e is the rms amplitude of the estuarine exchange flow, L is the length of the estuary defined as the distance from the ocean end of the domain to the upriver location where the tidally averaged bottom salinity drops to 5% of the oceanic value (32 psu), γ is a measure of the importance of stratification to the dynamics of the lateral circulation [see Eq. (3), within which we approximate the buoyancy frequency using the tidal-average, top-to-bottom density difference at the *thalweg*, $\Delta\rho(z)$, and we set ρ_o to 1025 kg m^{-3}, B to 1000 m, and H to the cross-channel average depth of 11.7 m], δ and v_{BL} are the boundary layer thickness and maximum current associated with the diffusive bottom boundary layer described in section 1, and max($|v_{LAT}|$) is the maximum lateral current observed over a tidal cycle (about 1 h after maximum flood) for each model run.

Run	A_v ($\times 10^{-4}$ m^2 s^{-1})	U_f (cm s^{-1})	$\Delta S(z)$ (psu)	U_e (cm s^{-1})	L (km)	γ	δ (m)	v_{BL} (cm s^{-1})	Max($\|v_{LAT}\|$) (cm s^{-1})
1	21.9	0.25	0.70	8.7	95.2	1.0	3.2	2.4	10.0
2	14.8	0.5	1.33	11.2	93.0	2.7	2.3	2.2	6.5
3	10.0	1.0	2.32	13.6	89.7	6.8	1.7	2.1	4.4
4	6.8	2.0	4.14	16.4	86.7	18	1.2	2.0	3.1
5	5.4	3.0	5.55	18.0	87.1	29	1.0	1.9	3.0
6	4.0	5.0	7.60	20.2	88.9	54	0.8	1.8	2.8
7	3.3	7.0	9.22	21.8	89.0	79	0.7	1.7	2.6

Temperature is set to a constant value of 4°C throughout the domain. At the ocean end, we use a salinity-dependent gradient condition to ensure that near-bottom salinity remains close to oceanic values on average. At the riverine end, the salinity is fixed at zero. Our model runs are insensitive to this boundary condition because the length of the estuary ($L \approx 90$ km)—that is, the upriver extent of the salinity intrustion—is always much less than the length of the domain (500 km).

We use a quadratric drag law to specify the bottom stress. Horizontal viscosities and diffusivities are set to zero and a free-slip boundary condition is applied at the side walls. Vertical eddy viscosity and diffusivity are set to the same constant value (Prandtl number set to 1). This idealization is not consistent with the spatially and temporally varying mixing observed in stratified, tidal, channel flows (Stacey et al. 1999; Geyer et al. 2000; Peters and Bokhorst 2001). However, using constant eddy coefficients allows us to make straightforward comparisons to the scalings of classic, analytic estuarine models, which assume constant eddy coefficients. Our intention is to use eddy coefficients that represent reasonable spatially and temporally averaged values so that we can shed some understanding on the dynamics of lateral flows in stratified estuaries and reveal the scaling relations more clearly.

A more realistic turbulence closure must be used to correctly parameterize the temporally and spatially varying interaction between tidally generated turbulence and stratification and its influence on the lateral circulation. However, we find that, for model runs in which a more realistic two-equation turbulence closure is used (see section 6f), the structure of the lateral circulation is qualitatively the same as that for the runs with constant eddy coefficients. This work is, thus, a first step and a reference case in the development of more realistic models that properly represent the spatial and temporal dependence of turbulence transfer.

The length of the estuary L, vertical stratification $\Delta S(z)$, and strength of the tidally averaged estuarine circulation U_e are all sensitively dependent on the freshwater outflow and the vertical eddy viscosities and diffusivities (Hansen and Rattray 1965; Chatwin 1976). In our model runs, we vary both the eddy viscosity (and diffusivity) A_v and the freshwater outflow U_f in a manner that allows the stratification to vary while keeping the tidal amplitude fixed and the length of the estuary roughly constant at 90 km (Table 1). This allows us to assess the influence of stratification on the lateral circulation, while keeping the along-channel density gradient, which is one of the key driving forces for the lateral circulation [Eq. (1)], roughly constant. The eddy viscosity was varied by almost an order of magnitude, consistent with temporal variations in eddy viscosity over a spring–neap cycle inferred from along-channel momentum budgets (Geyer et al. 2000) and from microstructure measurements (Peters and Bokhorst 2001) in a partially mixed estuary.

In the model runs, the top-to-bottom salinity difference at a midestuary location ($x \approx 45$ km) varied from 0.70 to 9.2 psu (Fig. 3a). This range in stratification has been observed in partially mixed estuaries over a spring–neap cycle in tidal amplitude (Geyer et al. 2000). While the along-channel baroclinic pressure gradient remains roughly constant (because the length of the estuary is roughly constant), the stratification increases with decreasing viscosity. As a consequence, the amplitude of the estuarine exchange flow increases with increasing stratification (Fig. 3b).

The along-channel structure of tidally averaged along-channel current $\overline{u}$ and salinity $\overline{S}$ is consistent with what is observed in partially stratified estuaries (Fig. 4). The estuarine exchange flow draws oceanic water into the estuary in the bottom portion of the water column, while the comparatively fresh water is driven out of the estuary near the surface.

3. Differential advection and the influence of stratification

We begin by describing results from model runs without rotation. The salient features of the lateral circulation

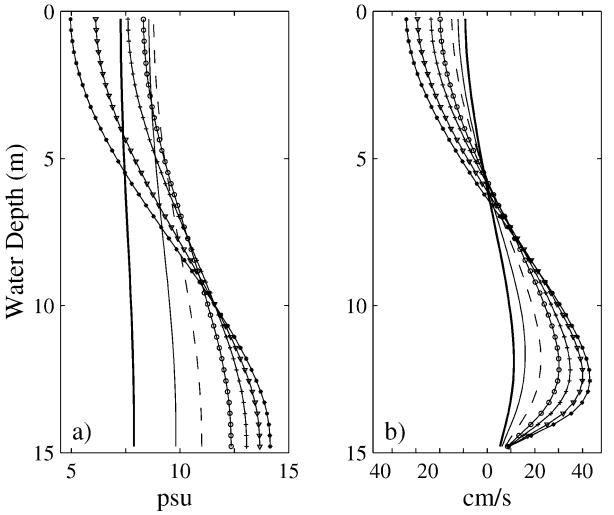

FIG. 3. Vertical profiles of tidally averaged (a) salinity and (b) along-channel current (u) at the *thalweg* and at a midestuary location for the seven model runs with varying eddy viscosity (A_v) and freshwater flow (U_f). The stratification and estuarine exchange flow increase as A_v is decreased (see Table 1 for the values of A_v and U_f used in these runs).

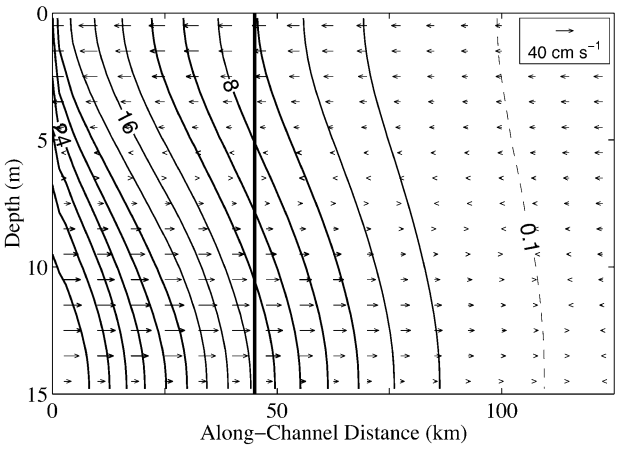

FIG. 4. Tidally averaged along-channel section of salinity (contours) and along-channel current (u, arrows) along the *thalweg* for the model run with $A_v = 4.0 \times 10^{-4}$ m^2 s^{-1} and $U_f = 5$ cm s^{-1} (Table 1). The contour interval is 2 psu except for the dashed contour, which indicates the landward extent of the salinity intrusion. The thick vertical line shows the midestuary location for this run. Note that the full domain of the model runs extends out to 500 km, well beyond the landward extent of the salinity intrusion.

at a midestuary location ($x \approx 45$ km), as it varies over a tidal cycle and under different levels of stratification, are summarized in Fig. 5. For the model run with weakest stratification (Table 1), two weak lateral circulation cells, symmetric about the channel axis, are apparent one hour after maximum ebb (Fig. 5a), with lateral currents divergent near the surface and convergent near the bottom. Maximum lateral currents are about 3.4 cm s^{-1}. Lateral salinity gradients are consistent with differential-advection forcing (saltier at the flanks than at the *thalweg*, Fig. 5b).

The maximum lateral circulation occurs an hour after maximum flood, when the lateral currents are much stronger than those during ebb, with maximum values of about 10 cm s^{-1} (Fig. 5c). Surface currents are convergent and bottom currents are divergent, consistent with the flood phase observations of Nunes and Simpson (1985). The lateral gradients in salinity are strong, with higher salinity in water at the *thalweg* than at the flanks (Fig. 5d), also consistent with differential-advection forcing of the lateral flow.

The influence of the lateral flow on the along-channel tidal currents is apparent during the flood phase of the tide (Fig. 5c). The lateral flow advects slow-moving, boundary-layer water into the interior of the channel at the surface. This results in strong lateral shear in the along-channel tidal currents, u_y, in the upper 5 m of the water column.

For the model run with strongest stratification, lateral currents are very weak (Figs. 5e,g). Cross-channel gradients in salinity are not apparent, except near the bottom where the diffusive boundary layer causes isohalines to be normal to the bottom (Figs. 5f,h).

One hour after maximum flood, a weak lateral circulation is apparent in the bottom half of the water column with downwelling at the *thalweg*, divergent flow in the bottom boundary layer, and maximum lateral currents of 2.6 cm s^{-1} (Fig. 5g). The combination of flood tidal currents and strong landward estuarine circulation near the bottom (Fig. 3b) leads to a subsurface maximum in the currents 4 m above the bottom.

To measure the strength of the lateral flow over a tidal cycle for the seven model runs with varying stratification, we calculate the cross-channel average of the lateral velocity amplitude, $\langle |v| \rangle$, at the midestuary location ($x \approx 45$ km):

$$\langle |v| \rangle = \frac{1}{A} \int |v| \, dA, \tag{7}$$

where $|v|$ is the absolute value of v and A is the cross-channel area.

For the weakly stratified estuary (Fig. 6, thick line), the maximum $\langle |v| \rangle$ is 3.9 cm s^{-1} and occurs at approximately 1 h after maximum flood. While the lateral circulation also peaks 1 h after maximum ebb, it is considerably weaker than the circulation after maximum flood.

The flood–ebb asymmetry in the strength of the lateral circulation is apparent in all seven model runs with varying stratification. The amplitude is highest 1–2 h after maximum flood (Fig. 6). However, the scale of the cross-channel flow decreases significantly with increasing stratification. We find that the maximum value of $\langle |v| \rangle$ over a tidal cycle is inversely proportional to the top-to-bottom salinity difference [$\langle |v| \rangle \sim \Delta S(z)^{-1}$].

We use the ratio of isopycnal tilting to differential advection, γ, as expressed in Eq. (3), to assess the im-

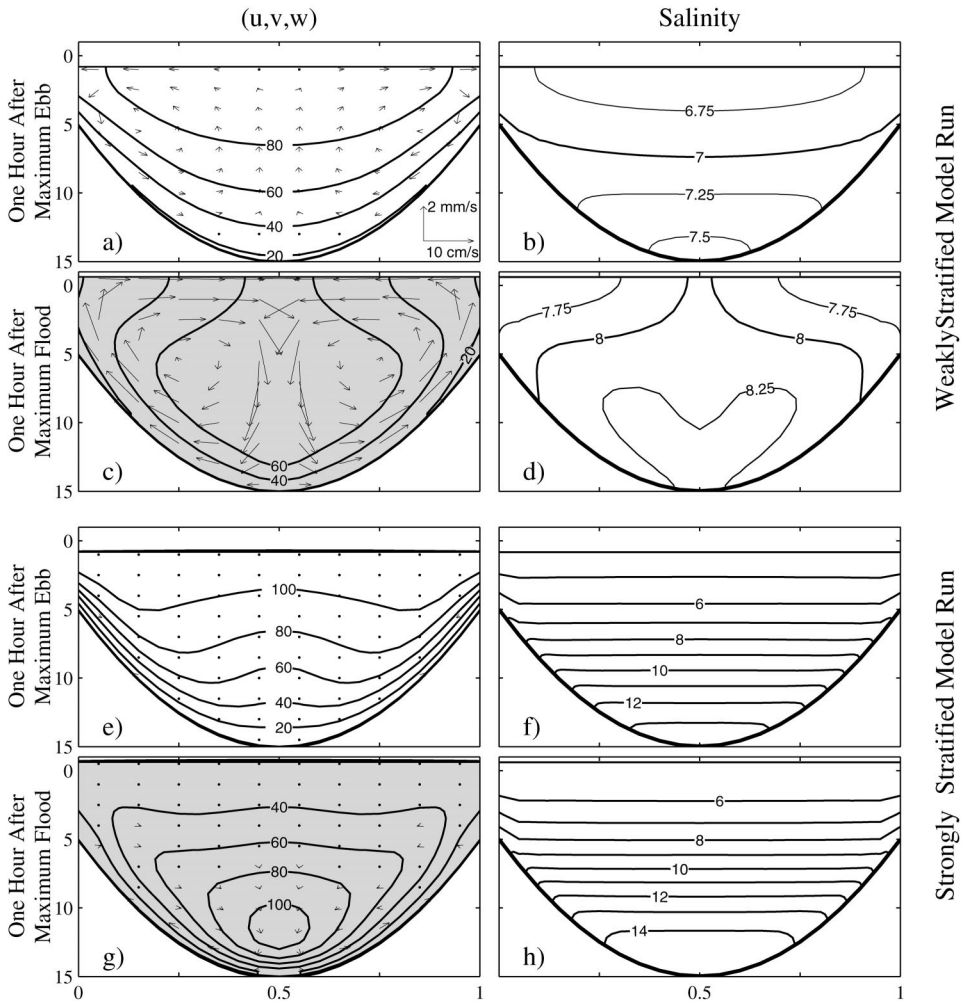

FIG. 5. Cross-sectional profiles of currents (u, v, w) and salinity for the (a)–(d) weakly stratified and (e)–(h) strongly stratified model runs without rotation (Table 1). Cross sections are at a midestuary location ($x \approx 45$ km) and are shown for 1 h after maximum flood and 1 h after maximum ebb. Along-channel currents are contoured with a 20 cm s^{-1} interval. Landward currents (directed out of the page) are shaded gray. Lateral currents are indicated by arrows at selected locations, with v and w scaled to match the aspect ratio of the channel cross sections. The salinity contour intervals are 1 psu (thick contours) and 0.25 psu (thin contours).

portance of stratification (Table 1). For the model run with the weakest stratification, the ratio is about 1 and suggests that stratification may play a role in the dynamics even when the tidally averaged, top-to-bottom density difference is only 0.63 kg m^{-3}. As the stratification increases, γ increases by nearly two orders of magnitude, consistent with the observed reduction in the strength of the lateral flow with increasing stratification.

4. Momentum balance

We now show the significance of the lateral circulation to the along-channel and cross-channel momentum budgets. When lateral flows are strong enough to advect water parcels a significant distance over a tidal time scale relative to 0.5 times the breadth of the channel (i.e., $4\langle|v|\rangle/\sigma B \gtrsim 1$), we expect lateral advection to be important in the estuarine dynamics. As shown previously, lateral advection of along-channel momentum is apparent during the flood phase for the weakly stratified model run (Fig. 5c). The scale of lateral excursions is greater than the half-breadth of the estuary at the peak of lateral flow (Fig. 6; see the scale on the right side of the figure). Therefore, we expect lateral advection to be an important term in the momentum budgets, at least for the weakly stratified estuary.

a. Momentum budget over a tidal cycle

The dominant balance in the along-channel momentum budget is between acceleration and the barotropic

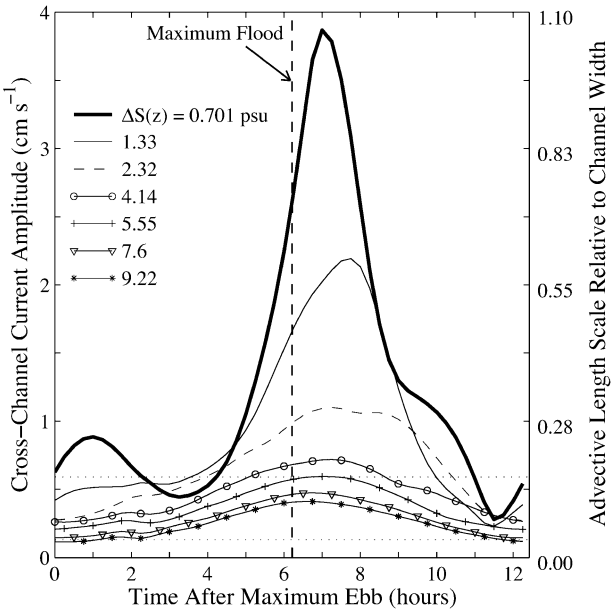

FIG. 6. Cross-channel average of cross-channel velocity amplitude, $\langle|v|\rangle = A^{-1}\int |v|\, dA$, vs time after maximum ebb at midestuary ($x \approx 45$ km) for model runs with varying stratification [top-to-bottom salinity difference, $\Delta S(z)$; see Table 1]. The right axis is a measure of the lateral advection distance relative to 0.5 times the channel width ($\equiv 4\langle|v|\rangle/\sigma B$; σ is the semidiurnal tidal frequency, and B is the channel width). A value of 1 indicates a cross-channel water parcel excursion of one-half of the channel width. The horizontal dotted lines indicate the value of $\langle|v|\rangle$ due to the diffusive boundary layer described in section 1d, as determined from simulations with the model channel with a linearly stratified fluid, initially at rest, that adjusts to the no-flux boundary condition. The upper line is for the weakly stratified model run, and the lower line is for the strongly stratified model run.

pressure gradient due to the barotropic tidal wave—that is, $u_t \approx -g\zeta_x$, where ζ is the sea surface elevation. We are interested in the higher-order momentum balance that drives the estuarine circulation and, therefore, compare the amplitude of $u_t + g\zeta_x$ with the rest of the terms in the momentum equation (Fig. 7a). As with the amplitude of the lateral circulation in the previous sections, we calculate the area average of the absolute value of each of the momentum equation terms ($\langle|\phi|\rangle$, where ϕ refers to any of the terms in the momentum equations). This allows us to assess the relative importance of the various terms in the momentum budget. Since the absolute value of the individual terms are area averaged, the curves in Fig. 7 do not sum to zero even though the momentum equations do balance.

In the along-channel momentum equation for the weakly stratified model run (Fig. 7a), lateral advection of along-channel momentum, $\langle|vu_y + wu_z|\rangle$ (thick line), is greatest about 1 h after maximum flood and plays a dominant role in the momentum balance at that time. The along-channel baroclinic pressure gradient, $\langle|\rho_o^{-1}\partial P_{BC}/\partial x|\rangle$, is roughly constant over a tidal cycle, with only a slight tidal modulation. This is because the along-channel density gradient is roughly constant over time and independent of x at the midestuary location. Vertical stress divergence, $\langle|A_v u_{zz}|\rangle$, and $\langle|u_t + g\zeta_x|\rangle$ vary significantly over a tidal cycle. Along-channel advection, $\langle|uu_x|\rangle$, is negligible at all times because along-channel gradients in u are weak.

In the cross-channel direction (Fig. 7b), terms in the momentum budget are comparatively weak except for the 2-h period when the lateral flow is strong, centered at about 1 h after maximum flood. At this time, the forcing by the lateral pressure gradient, $\langle|P_y/\rho_o|\rangle$, is clearly evident, indicating that differential advection is the dominant forcing mechanism. This forcing is balanced by lateral advection, vertical stress divergence, and, to a lesser degree, acceleration.

For the strongly stratified estuary in the along-channel direction, $\langle|u_t + g\zeta_x|\rangle$, the baroclinic pressure gradient, and vertical stress divergence are dominant over most of the tidal cycle (Fig. 7c). One hour after maximum flood, lateral advection also becomes significant, despite the small amplitude of the lateral circulation. However, it is less than one-quarter of the value of $\langle|vu_y + wu_z|\rangle$ of the weakly-stratified model run. During this period of the tidal cycle, weak downwelling acts across the strong vertical shear at the base of the core of the tidal currents near the bottom of the water column (Figs. 5g), resulting in a comparatively large advective acceleration, wu_z, there. Lateral advection throughout most of the channel cross-section, however, is weak. In the cross-channel direction, cross-channel pressure gradient and vertical stress divergence dominate the momentum balance (Fig. 7d), and all other terms are insignificant. Cross-channel acceleration is insignificant apparently because the cross-channel currents are concentrated in a thin diffusive boundary layer ($\delta < 1$ m) at the channel bottom. The diffusive time scale ($\delta^2/A_v \sim 30$ min) for this boundary layer is significantly smaller than the acceleration time scale ($\sigma^{-1} \sim 2$ h).

b. Tidally averaged along-channel momentum budget

As expected, the tidally averaged along-channel current $\overline{u}$ has the structure of an estuarine exchange flow with oceanward currents near the surface and landward currents near the bottom (Figs. 8a,c). For the weakly stratified estuary, a tidally averaged lateral circulation persists (arrows in Fig. 8a) because of the flood–ebb asymmetry in the lateral flow (strong during flood and weak during ebb). The maximum current of this tidally-averaged lateral flow is about 2 cm s^{-1} with convergent surface flow and divergent bottom flow.

The tidally averaged lateral advection term acts as an oceanward driving force for surface waters and a landward driving force for bottom waters (Fig. 8b). This is because the mean lateral circulation is dominated by the flow during the flood phase, which advects water with comparatively high oceanward momentum into the surface layer and water with comparatively high landward momentum near the bottom of the channel (Fig. 5c).

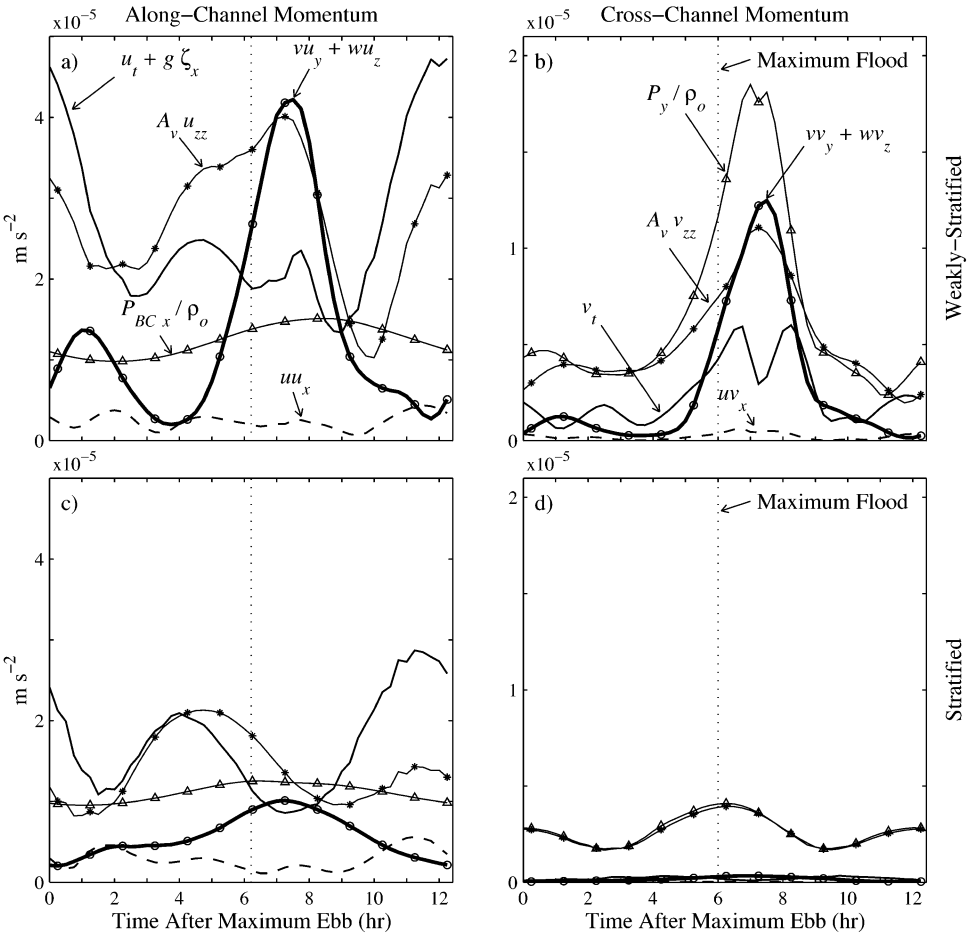

FIG. 7. Cross-sectional averages of the absolute value of the terms in the (a), (c) along-channel and (b), (d) cross-channel momentum equations over a tidal cycle at a midestuary location ($x \approx 45$ km) for the weakly stratified and strongly stratified model runs without rotation (Table 1). The vertical dotted line indicates the time of maximum flood. In (a) and (c), the acceleration and barotropic pressure gradient are combined ($\langle | u_t + g\zeta_x | \rangle$) to remove the dominant balance associated with the barotropic tidal wave. Note that the curves in the figure do not balance because the absolute values of the individual momentum terms were area averaged. Note that the *y*-axis scales for the along-channel and cross-channel panels are different.

Consequently, tidally averaged lateral advection acts as a driving force for the estuarine circulation, augmenting the along-channel pressure gradient force.

Because of the smaller eddy viscosity of the strongly stratified model run, the tidally averaged estuarine exchange circulation is stronger than for the weakly stratified run (cf. Figs. 8a and 8c). The tidally averaged lateral circulation, however, is much weaker, though downwelling is apparent in the landward core of the exchange flow. This downwelling tends to push the landward portion of the exchange flow downward and increase the shear in the landward currents, resulting in a large tidally averaged lateral advection term near the bottom (Fig. 8d). However, lateral advection is weak throughout most of the channel cross section.

We now compare the significance of tidally averaged lateral advection to the rest of the terms in the tidally averaged along-channel momentum equation. For all model runs, lateral advection, pressure gradient, and vertical stress divergence are significant (Fig. 9). Acceleration, $\overline{u_t}$, and along-channel advection, $\overline{uu_x}$, are insignificant. The notable result is that lateral advection is comparable to or larger than the pressure gradient for the weakly stratified estuary. This is particularly evident off the channel axis (Fig. 9b) because the symmetry of the channel causes the cross-channel flow to be stongest off the channel axis (Figs. 5c and 8b). For the strongly stratified model run, tidally averaged lateral advection is insignificant in the upper part of the water column, and the dominant balance there is between the pressure gradient and vertical stress divergence (Figs. 9c,d). The effect of downwelling on the momentum balance is most apparent near the bottom of the water column at the *thalweg*. There, lateral advection tends to enhance shear in the bottom boundary layer, resulting in a significantly enhance stress divergence.

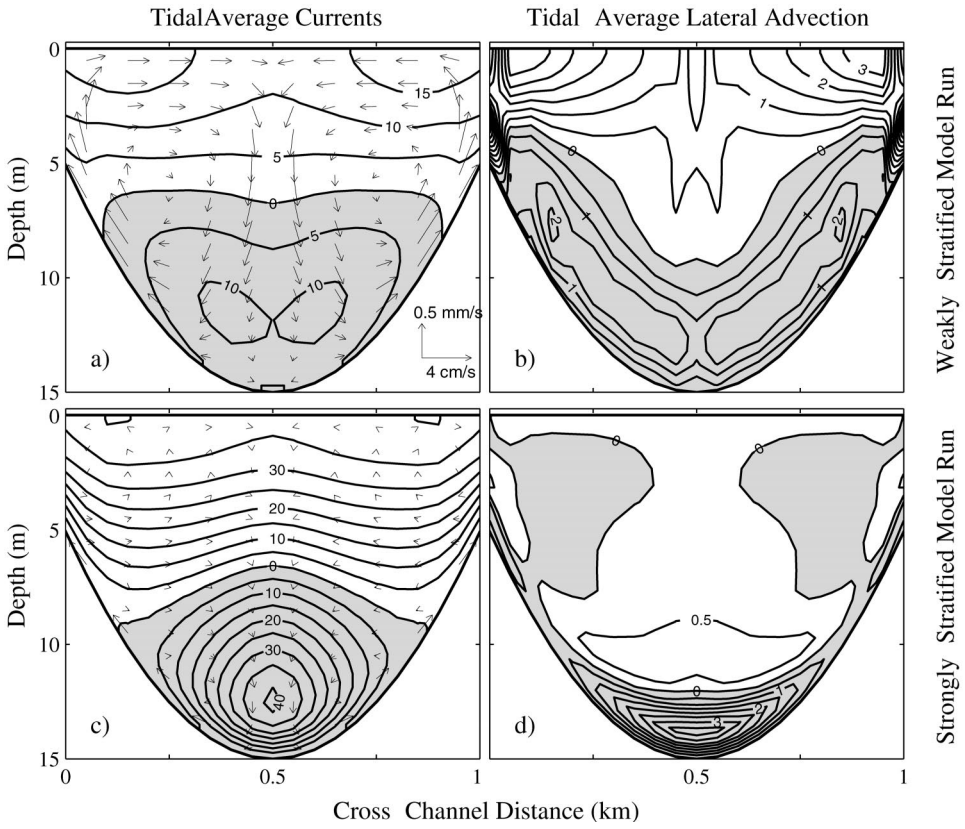

FIG. 8. Cross-channel sections of tidal-average currents ($\overline{u}$, $\overline{v}$, $\overline{w}$) and lateral advection of along-channel currents ($\overline{vu_y} + \overline{wu_z}$) for the (a), (b) weakly stratified and (c), (d) strongly stratified model runs (Table 1). The overbar indicates averaging over a tidal cycle. Landward currents (directed out of the page) and lateral advection that tends to accelerate landward currents are shaded gray. Lateral currents are indicated by arrows at selected locations, with v and w scaled to match the aspect ratio of the channel cross sections. Lateral advection is contoured in units of 10^{-5} m s^{-2}.

5. Influence of rotation

When rotation is included in the model, the asymmetry in the circulation relative to the channel axis is broken (Fig. 10, $f = 1 \times 10^{-4}$ s^{-1}). The Coriolis term, fu, is a dominant term in the cross-channel momentum equation that must be balanced by a cross-channel pressure gradient, as is evident by the tilting isohalines in Figs. 10b, 10d, 10h, and 10j.

At 1 h after maximum ebb, for the weakly stratified model run, the lateral flow is dominated by a circulation cell driven by Ekman forcing (Fig. 10a). This cell is strongest on the right side of the channel (when facing the ocean in the Northern Hemisphere), with maximum lateral currents of 3.6 cm s^{-1}. Weak differential-advection forcing is made apparent by the laterally divergent flow at the surface and a second, comparatively weak, circulation cell that flows counter to Ekman forcing on the left side of the channel.

At slack tide after ebb (3.25 h after maximum ebb), the lateral circulation is dominated by a single circulation cell across the channel (Fig. 10a). The near-bottom (landward) currents drive an Ekman flow to the right bank. In addition, the isopycnals, which were tilted and approximately in thermal wind balance with the ebb currents 2.25 h earlier (Fig. 10b), slump back toward level during slack tide, providing an additional driving force for the lateral circulation seen in Fig. 10c. Maximum lateral currents are 4.6 cm s^{-1}.

Differential advection dominates over Ekman forcing one hour after maximum flood, when maximum lateral currents are over 10 cm s^{-1}. The two-cell circulation pattern and the salinity field are nearly symmetric about the channel axis (Figs. 10e and 10f).

Like the case without rotation, lateral circulation is very weak at 1 h after maximum ebb (not shown in figure) and slack tide after ebb for the model run with strongest stratification (Fig. 10g). Isohalines tilt downward to the right in response to Ekman forcing. One hour after maximum flood, the subsurface maximum in the along-channel currents is to the left of the channel axis (Fig. 10i). The lateral circulation near the bottom is enhanced on the right side of the channel, and maximum lateral currents are 4.6 cm s^{-1}. Isohalines remain predominantly tilted downward to the right because the

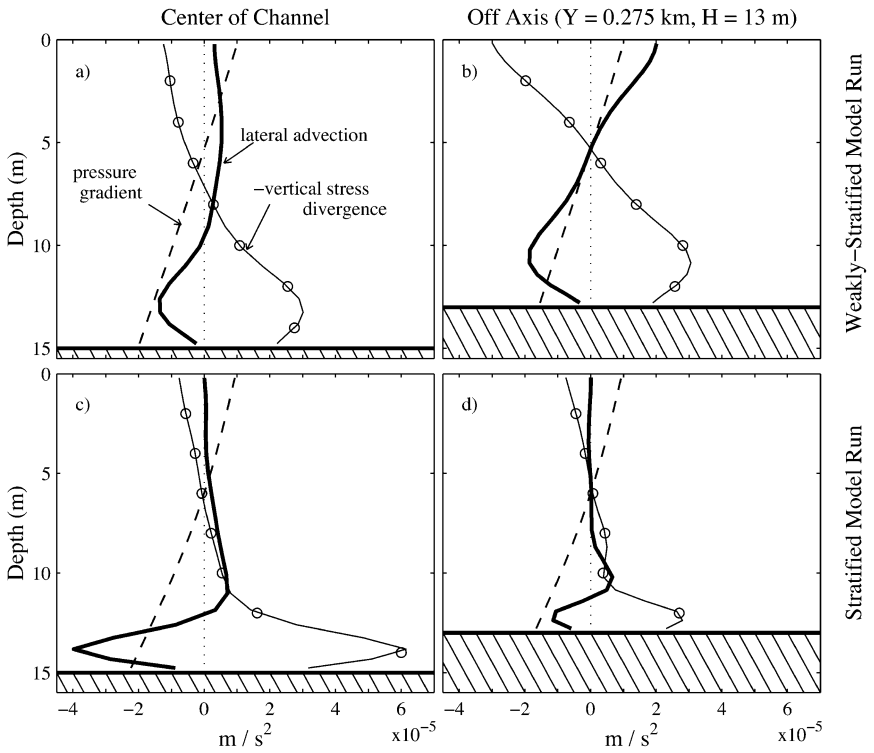

FIG. 9. Vertical profiles of the three dominant tidally averaged along-channel momentum terms at the *thalweg* and off the channel axis at a depth of 13 m for the (a), (b) weakly stratified and (c), (d) strongly stratified model runs (Table 1). Pressure gradient = $\overline{P}_x/\rho_o$, negative vertical stress divergence = $-A_v\overline{u}_{zz}$, and lateral advection = $\overline{vu}_y + \overline{wu}_z$, where the overbar indicates averaging over a tidal cycle. Thick, horizontal lines indicate the channel bottom.

sign of the vertical shear in the along-channel currents does not change relative to ebb tide throughout much of the water column (above the subsurface maximum, the shear is positive, with increasing currents in the oceanward sense toward the surface), and the tilt of the isohalines, in accordance with the thermal wind balance, is the same for flood and ebb.

With weak stratification, the peak of strong lateral circulation after flood tide persists with rotation added to the dynamics (Fig. 11). With rotation, a second peak in lateral flow, due to time-dependent Ekman forcing, occurs at about slack after ebb. For strong stratification, adding rotation to the dynamics increases the level of the lateral flow slightly throughout the tidal cycle.

6. Discussion

a. Driving mechanisms of lateral circulation

Both differential advection and Ekman forcing drive significant lateral flows. However, the lateral circulation due to the diffusive boundary layer, which is confined to a bottom boundary layer, is comparatively insignificant as determined by analytical theory [Eqs. (5) and (6); Table 1] and confirmed by simulations with our channel domain, with a linearly stratified fluid that is initially at rest and adjusts to the no-flux boundary condition. The level of $\langle |v| \rangle$ associated with the diffusive boundary layer is well below the level of $\langle |v| \rangle$ because of differential advection for most of the tidal cycle (see dotted lines in Fig. 6).

b. Flood–ebb asymmetry

For the model run with weakest stratification, lateral flow is about 4 times as great during flood tide as during ebb (Fig. 6). This asymmetry is due, in part, to the interaction between the along-channel tidal currents and the lateral flow itself. During flood tides, the lateral flow is convergent at the surface and divergent near the bottom. This circulation pattern advects slowly moving tidal boundary layer water into the interior of the channel and enhances the lateral shear in u (Fig. 5c). The enhanced lateral shear increases the differential advection of the along-channel density gradient and, thus, enhances the mechanism that drives the lateral circulation [see Eq. (1)]. However, the growth of the lateral circulation due to this positive feedback must be limited because, if the lateral circulation becomes too strong (e.g., if water parcels were advected completely around a circulation cell during the period of a flood tide), the transverse exchange of momentum would tend to ho-

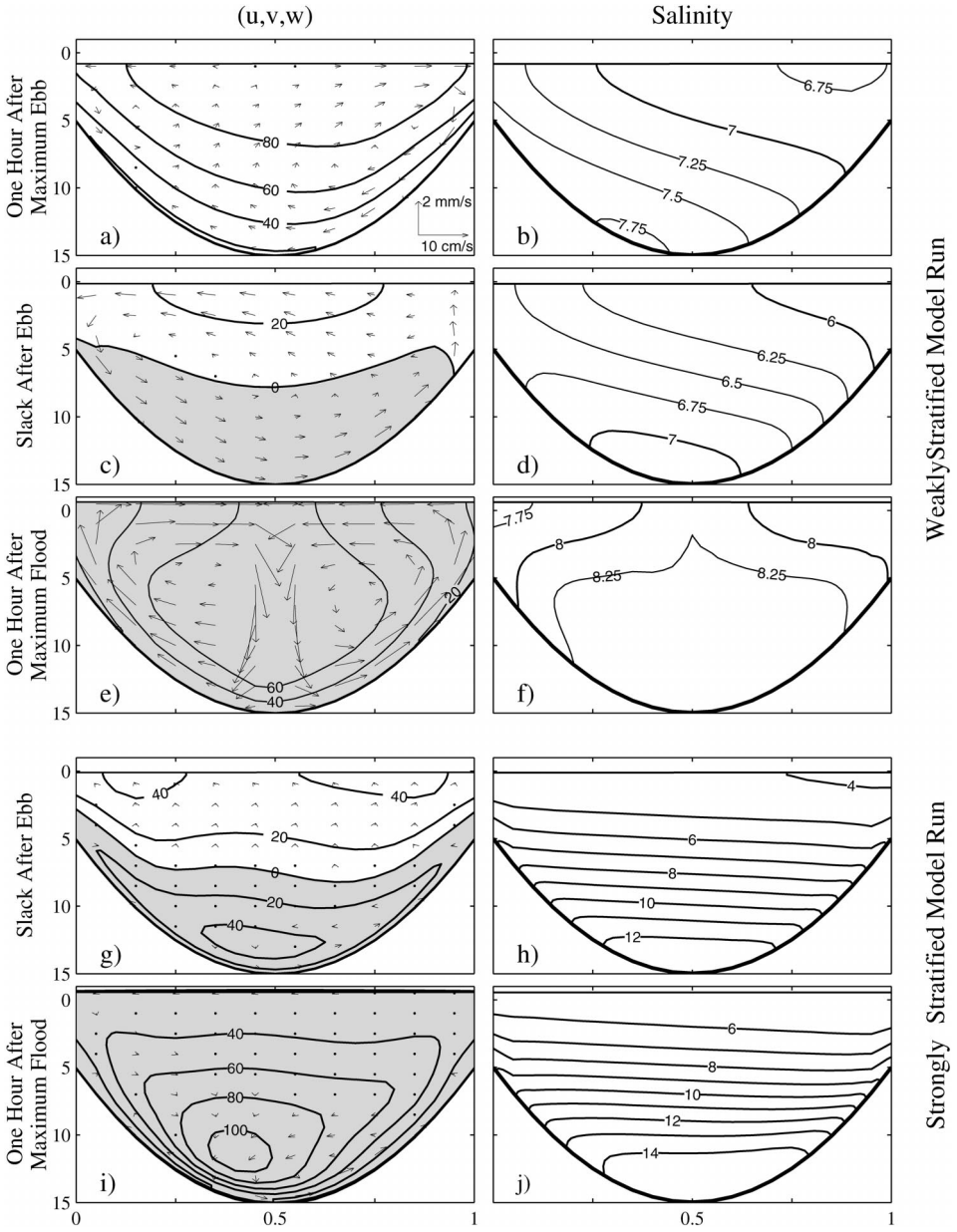

FIG. 10. Similar to Fig. 5 but for model runs with rotation ($f = 1 \times 10^{-4}$ s^{-1}). Cross-channel profiles are shown for 1 h after maximum ebb (weakly stratified run only), slack tide after ebb (3.25 h after maximum ebb), and 1 h after maximum flood.

mogenize the tidal currents laterally and thus suppress the differential-advection driving mechanism.

During ebb, the lateral flow is divergent at the surface and convergent near the bottom. This pattern tends to draw interior fluid toward the lateral boundaries, flatten the tidal current isotachs, and reduce the lateral shear in u (Fig. 5a). This tends to reduce differential advection and suppress the lateral circulation.

This effect is illustrated in Fig. 12. Lateral shear in the along-channel tidal currents, u_y, in the interior of the channel is more than 4 times as large 1 h after maximum flood as during the ebb phase of the tide (Fig. 12a). Consequently, the cross-channel gradient in density (Fig. 12b) and the lateral pressure gradient which drives the lateral circulation (Fig. 7b) are much greater during the flood than during the ebb phase of the tide.

Time-varying stratification also plays a role in the asymmetry of the lateral circulation over a tidal cycle. During flood tide, vertical shear in tidal currents, u_z, tends to strain the along-channel density gradient in a sense that reduces stratification (Simpson et al. 1990; Stacey et al. 2001; Nepf and Geyer 1996). During ebb,

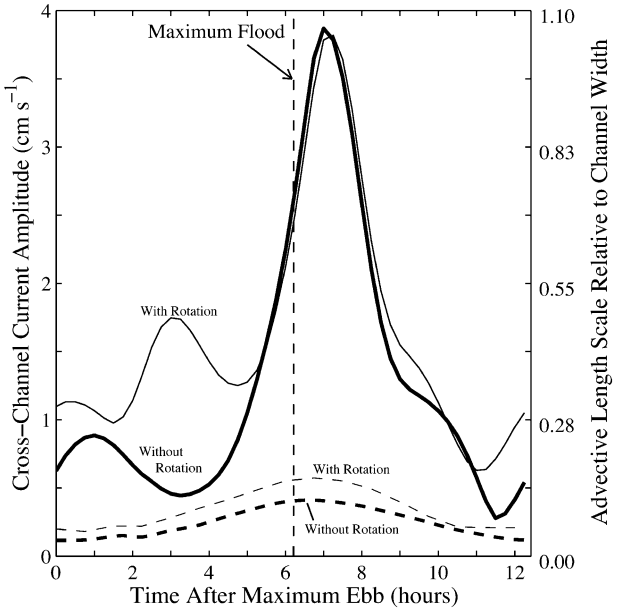

FIG. 11. As in Fig. 6 but comparing $\langle |v| \rangle$ for model runs with (thin lines) and without (thick lines) rotation ($f = 1 \times 10^{-4}$ s^{-1}). Curves are shown only for the model runs with the weakest (solid lines) and strongest (dashed lines) stratification (Table 1).

straining of the density field due to u_z tends to enhance vertical stratification. For our well-mixed model run, the top-to-bottom density difference ranged from 0.20 to 0.85 kg m^{-3} over a tidal cycle with weakest stratification at the same time as maximum lateral flow (1 h after maximum flood; Figs. 5c,d). Thus, the importance of stratification to the dynamics of the lateral circulation, as expressed by γ in Eq. (3), varies over a tidal cycle (Fig. 12d). During ebb tide, $\gamma \approx 1.25$, and stratification is predicted to suppress the lateral flow. One hour after flood tide, γ drops to about 0.3, suggesting that stratification has little impact on the lateral circulation at that phase of the tidal cycle.

c. Forcing of the subtidal estuarine circulation

The dominant momentum balance for the estuarine exchange circulation (tidally averaged, along channel) is often assumed to be between the along-channel pressure gradient and the vertical stress divergence (Hansen and Rattray 1965; Chatwin 1976; Smith 1976; Wong 1994; Trowbridge et al. 1999; Geyer et al. 2000). However, in our model runs, lateral advection is just as large or larger than the pressure gradient under weakly stratified conditions (Fig. 9). The advective term persists after averaging over a tidal cycle because of the asymmetry in the lateral flow between flood and ebb. On average, this advection of the tidal currents results in a rectified oceanward flow at the surface and a landward flow near the bottom. That is, the lateral circulation removes energy from the barotropic tide and pumps it into the tidally averaged estuarine circulation.

Thus, in this idealized estuary, there are two terms that drive the estuarine exchange flow—the along-channel pressure gradient and tidally averaged lateral advection—and the exchange flow will be stronger than what is predicted by the theory of Hansen and Rattray (1965). This is observed in our model runs (Fig. 13), for which the strength of the exchange circulation falls off more slowly with vertical eddy viscosity ($u_e \sim A_v^{-0.47}$) than the scaling of Hansen and Rattray (1965) ($u_e \sim A_v^{-1}$). Under forcing conditions different than those used here, additional mechanisms may also act to drive the estuarine exchange flow (e.g., residual currents forced by a large amplitude tide; Ianniello 1977, 1979).

The estuarine exchange flow modeled here varies predominantly in the vertical direction, with oceanward flow in a surface layer and landward flow in a bottom

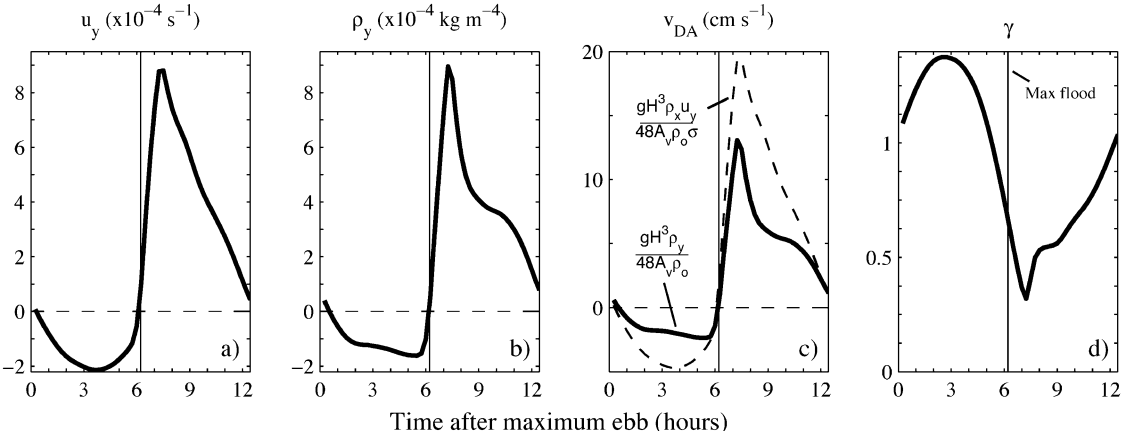

FIG. 12. (a) Lateral shear in along-channel tidal currents u_y, and (b) cross-channel density gradient ρ_y, averaged over a region in the interior of the channel (y = 200–500 m, $z \approx 0$ to 3.5 m below the surface) at a midestuary location ($x \approx 48$ km). (c) Strength of differential advection forced lateral circulation, v_{DA}, estimated from the scalings in Eq. (1). (d) Here γ is a measure of the importance of stratification to the dynamics of lateral circulation [see Eq. (3)]. The thin vertical line in (a)–(d) indicates the time of maximum flood. All plots are for the model run with weakest stratification (Table 1).

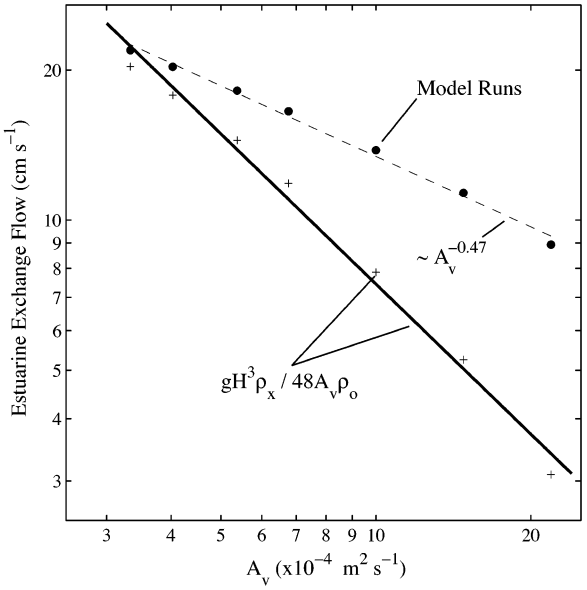

FIG. 13. Estuarine exchange flow vs vertical eddy viscosity. The solid line is the scaling for the exchange flow assuming a dominant balance between along-channel pressure gradient and vertical stress divergence (Hansen and Rattray 1965), using the mean water depth and mean along-channel density gradient of the seven model runs (Table 1). The pluses indicate the Hansen and Rattray scaling, using the actual along-channel density gradients (slightly different for each model run). The dots indicate the rms exchange flow across the channel observed in the seven model runs at a midestuary location ($x \approx$ 45 km).

layer (Figs. 8 and 14). This contrasts the linear analytical model, which assumes an along-channel momentum balance between vertical stress divergence and an along-channel baroclinic pressure gradient (Fischer 1972; Wong 1994; Friedrichs and Hamrick 1996) and predicts that, with modest variations in cross-channel bathymetry, the estuarine exchange flow varies predominantly in the lateral direction, with oceanward flow in shallow regions and landward flow in the *thalweg* of the estuary. However, such a linear model does not take into account differential advection that drives lateral variations in density and a lateral circulation (Smith 1976, 1980, 1996) nor the feedback of the lateral circulation onto the density field and the along-channel circulation (Scott 1994; the modeling presented here). These effects tend to increase vertical stratification of both the density field and the along-channel circulation and reduce lateral variability.

Presumably, as the width of the estuary increases, the influence of the lateral circulation on the along-channel circulation is reduced. As $H/B \rightarrow 0$, the time required for the lateral flow to advect a water parcel significantly across the estuary becomes longer than the time scale of vertical mixing, and the structure of the estuarine exchange flow and density field varies more laterally rather than vertically. The relationship between the feedback of the lateral flow onto the estuarine circulation and how it shapes the lateral and vertical structure of the density field and estuarine circulation of estuaries with varying widths needs to be explored further.

d. Rotation and cross-channel asymmetry

For model runs with rotation, tidally averaged stratification and estuarine circulation are asymmetric about the channel axis due to the dominant cross-channel geostrophic balance (Figs. 14a,c). The asymmetry of the estuarine circulation leads to an asymmetric tidally averaged lateral circulation with stronger near-bottom flow to the right flank of the channel (when looking toward the ocean in the Northern Hemisphere, Figs. 14b,d). This asymmetry may be a mechanism for driving asymmetric channel profiles in estuaries. The enhanced near-bottom flow to the right side of the channel could preferentially transport suspended sediment to the right, which over time could lead to shallow shoals on the right and the *thalweg* shifted to the left. This hypothesis could be tested by comparing channel asymmetry in Northern and Southern Hemisphere estuaries.

e. Comparison with observations

We briefly describe some observations of the lateral circulation taken at a straight reach of the Hudson River estuary about 4 km north of the George Washington Bridge and 22 km north of the Battery on Manhattan Island, New York [see Geyer and Nepf (1996) for a map of the estuary]. Acoustic Doppler current profiler (ADCP) and CTD measurements were made at a location to the right of the *thalweg* (when looking toward the ocean) over a 43-day period in the spring of 2002. Lateral currents and stratification for spring and neap tidal conditions are summarized in Fig. 15. During spring tides (weak stratification) lateral currents are strong (10–15 cm s^{-1}) during flood tide. The circulation had a mode-1 vertical structure with near bottom currents directed toward the flank and surface currents directed toward the interior (Fig. 15a), consistent with the modeling done here. Lateral currents were considerably weaker during ebb.

Flood tide lateral currents (~7 cm s^{-1}) were also much stronger than ebb tide lateral currents during neap tidal conditions (strong stratification, Fig. 15c). However, unlike the mode-1 structure predicted by the model runs, flood tide lateral currents had a mode-2 vertical structure with surface and bottom currents directed toward the flank and currents at the base of the pycnocline directed toward the *thalweg* (Fig. 15c).

The lateral advective length scale relative to the channel width ($2|v|/\sigma B$, with $|v| = 10$ cm s^{-1} and B = 1.6 km) is about 1, suggesting that water parcels may be significantly advected across the Hudson channel during flood tide. This strongly suggests that lateral advection is a significant term in the along-channel momentum budget during flood tide. The observed flood/

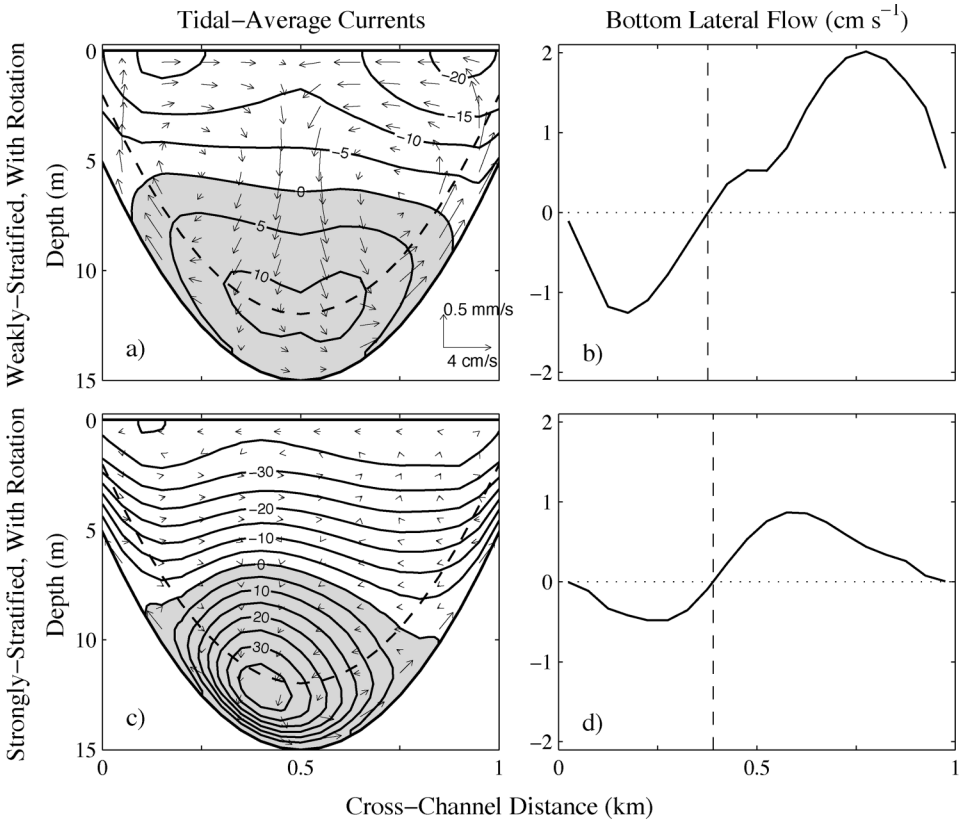

FIG. 14. (a), (c) Cross-channel sections of tidal-average currents ($\overline{u}$, $\overline{v}$, $\overline{w}$), and (b), (d) tidal-average lateral current averaged over the bottom 3 m of the water column [below the dashed line in (a) and (c)]. Rotation is included in these model runs ($f = 1 \times 10^{-4}$ s^{-1}). Landward currents (directed out of the page) are shaded gray. Lateral currents are indicated by arrows at selected locations, with v and w scaled to match the aspect ratio of the channel cross sections. The vertical dashed lines in (b) and (d) indicate the cross-channel location where the near-bottom lateral currents are zero.

ebb asymmetry in the strength of the lateral flow also suggests that the effects of lateral advection will not average to zero over a tidal cycle and that lateral advection may be an important term in the tidally averaged, estuarine momentum balance. Quantitative estimates of the terms of the momentum equations is beyond the scope of this paper, but further investigation is warranted.

Whereas the observations during conditions of weak stratification are consistent with the model results, the strong stratification observations have much stronger lateral circulation than predicted by the constant-eddy-coefficient numerical modeling presented here. We believe this difference between our strongly stratified model runs and the observed Hudson River estuary lateral circulation during neap tides is due to differences in the vertical structure of stratification. In the model runs, the channel was stratified at all depths (Figs. 3a and 5f,h), whereas, in the Hudson, a strong pycnocline separated comparatively well-mixed surface and bottom layers (Fig. 15d). With this vertical structure of stratification, a mode-2 circulation pattern can be driven without significantly tilting the strong pycnocline. These differences in the observed and modeled lateral circulation underscore the importance of properly parameterizing the temporal and spatial structure of mixing in order to understand the important feedback between lateral flows, mixing, and stratification.

f. Model runs with the k–ω turbulence closure

Last, we briefly describe the lateral circulation obtained from model runs in which we employ the k–ω two-equation turbulence closure (Wilcox 1998) using the stability functions of Kantha and Clayson (1994). This parameterization has been shown to yield quantitatively similar results to other popular two-equation turbulence closures (Warner et al. 2004), such as the Mellor–Yamada level-2.5 (Mellor and Yamada 1982) and the k–ϵ (Burchard and Baumert 1995). Two model runs are described here. For both runs, a freshwater velocity U_f of 5 cm s^{-1} is imposed. The tidal amplitude is set at 1 m s^{-1} for the first run and 0.7 m s^{-1} for the second, resulting in significantly different levels of stratification for the two runs (Fig. 16).

The strength of the lateral circulation is comparable

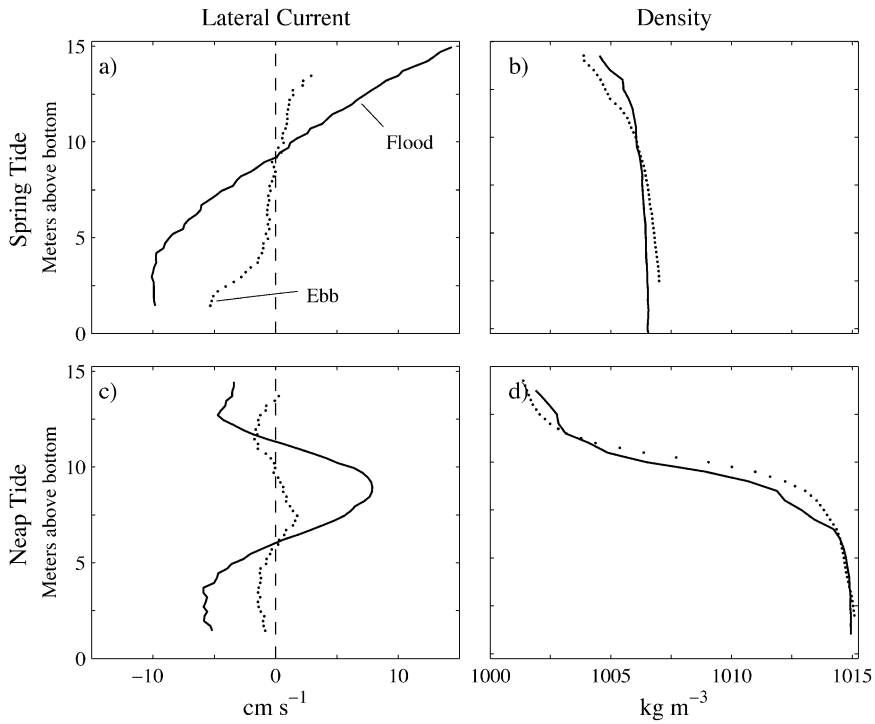

FIG. 15. (a), (c) Lateral currents and (b), (d) density vs depth at a location to the right of the *thalweg* (when looking toward the ocean) at spring and neap tidal conditions in the Hudson River estuary during the spring of 2002. The currents and the density fields were averaged over a 1-h period centered on maximum flood (solid line) and maximum ebb (dotted line). Negative currents are directed toward the right flank (when looking toward the ocean) and positive currents are toward the *thalweg*.

to that for the runs with constant eddy coefficients (cf. Figs. 5 and 16). The strong asymmetry in the lateral circulation (strong 1 h after flood and weak 1 h after ebb) is also apparent in the runs using the k–ω closure. For the weakly stratified run (Figs. 16a–d), the influence of the lateral circulation on the along-channel tidal currents and the salinity field is qualitatively similar to that in the weakly stratified run with constant eddy coefficients (Figs. 5a–d). Lateral advection is strong in the tidally averaged, along-channel, momentum budget and, as in the run with constant eddy coefficients, acts as a significant driving term for the estuarine circulation.

Unlike the strongly stratified model run with constant eddy coefficients, for which much of the water column was stratified (Figs. 5f,h), the stratified model run with the k–ω closure had a weakly stratified tidal boundary layer below a strong halocline (Figs. 16f,h), more closely resembling the vertical structure of stratification observed in the Hudson River during neap tides (Fig. 15d). Lateral currents were suppressed in the halocline and above. Unlike the constant eddy coefficient run, a significant lateral circulation was present at 1 h after maximum flood in the weakly stratified region below the halocline (Fig. 16g; $H < 4$ m) with flow toward the flank near the bottom and flow toward the *thalweg* just below the halocline. Consequently, lateral advection was a significant term in the along-channel momentum budget at 1 h after maximum flood and in the tidally averaged along-channel momentum budget in the region below the halocline. A similar circulation pattern below the pycnocline was also apparent in the Hudson River observations (Fig. 15c). However, the observed flow toward the flank above the halocline in the observations, did not occur in the k–ω model run.

7. Summary and conclusions

In this numerical study, we have shown that differential-advection and Ekman-forced lateral circulation can play an important role in cross-channel and along-channel momentum balances, particularly for weakly stratified estuaries. Feedbacks between the lateral flow, along-channel tidal currents, and time-varying stratification over a tidal cycle are important to the dynamics of the lateral flow and the tidally averaged estuarine circulation. In the tidally averaged, along-channel dynamics, lateral advection of momentum acts as an additional driving force for the estuarine circulation that can be as large as the along-channel pressure gradient. Therefore, it should not be neglected in estimates of the momentum budget in estuaries, as is typically done (Geyer et al. 2000).

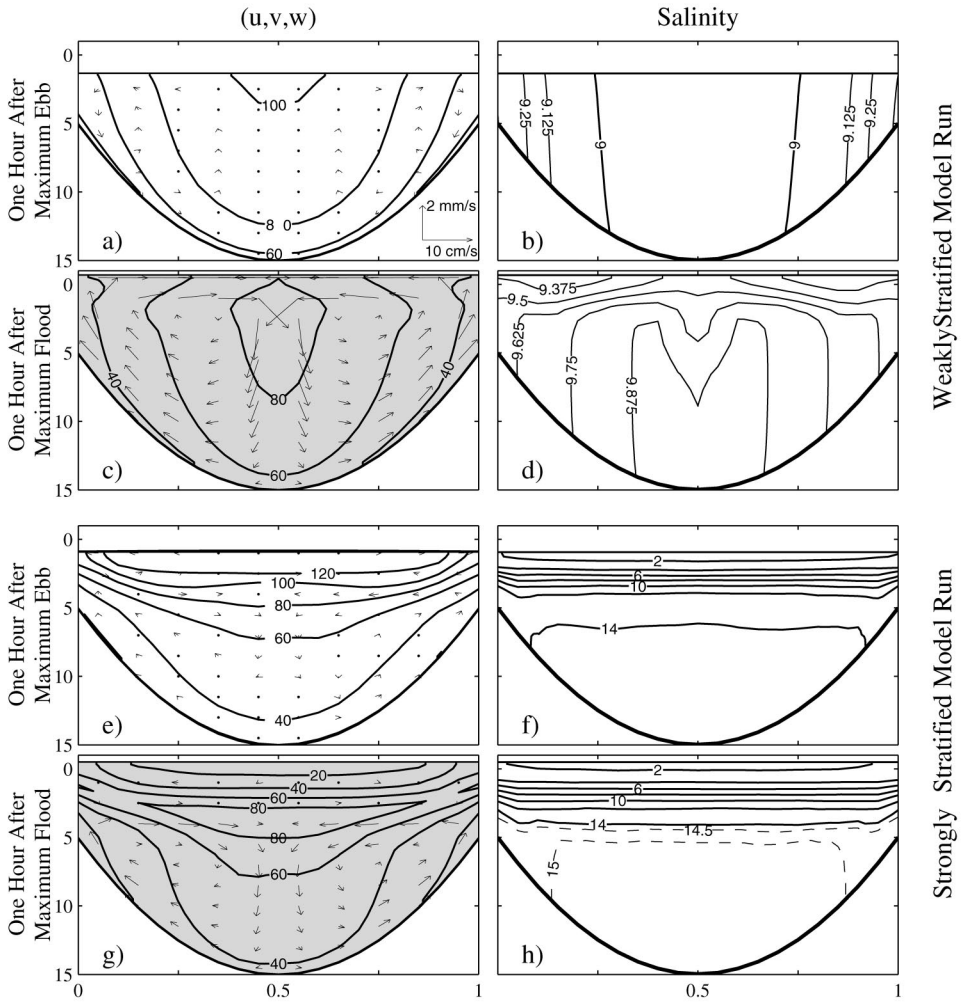

FIG. 16. As in Fig. 5 except the k–ω turbulence closure is employed instead of constant eddy coefficients. (a)–(d) $U_f = 5$ cm s^{-1}, and the tidal amplitude is 1 m s^{-1}. (e)–(h) $U_f = 5$ cm s^{-1}, and the tidal amplitude is 0.7 m s^{-1}. For the strongly stratified model run, salinity contour intervals are 2 psu (solid lines) and 0.5 psu (dashed lines for $S > 14$ psu).

Time-dependent lateral Ekman circulation can also be significant. Averaged over a tidal cycle, the combination of differential advection and Ekman forcing leads to an asymmetric lateral circulation pattern across the channel. This asymmetry may drive asymmetric lateral sediment transport which may ultimately lead to a prefered asymmetric channel shape in straight estuaries (shallow flanks to the right and deep channel to the left when looking toward the ocean).

The stratification in partially mixed estuaries can vary significantly over a spring–neap cycle. Our modeling suggests that the structure of the lateral circulation will, therefore, change significantly over a spring–neap cycle. The modeling with constant eddy coefficients also suggests that the amplitude of the cross-channel flows will be much greater during springs than during neaps. However, unlike our model runs with constant eddy coefficients, observations in the Hudson suggest that the lateral circulation can remain strong during neap tides, but its vertical structure differs from the lateral flow observed during spring tides. This is further supported by runs made with the k–ω turbulence closure. This points to a limitation in our modeling and underscores the importance of properly paramaterizing the vertical and temporal structure turbulent mixing in numerical studies of estuaries.

The idealized estuary used in this numerical study is straight and prismatic, and has a simple, symmetric parabolic cross section that does not vary along the channel. Yet, despite this simplicity, strong and complex lateral flows are generated, and these flows are important to the overall estuarine dynamics. This study, therefore, represents a starting point for further investigations of the role of lateral circulation in more realistic estuarine

domains that might include, for example, channel curvature, large amplitude tides, realistic turbulence closures, and more complicated and varied channel geometries and tidal regimes.

Acknowledgments. The authors are indebted to Rob Hetland and John Warner for their help in setting up the ROMS simulations. Thanks are given to Clint Winant, Kipp Shearman, and two anonymous reviewers for their insightful review of the manuscript. This work was supported by National Science Foundation Grant OCE99-06787.

APPENDIX

Ekman-Forced Lateral Flow in a Homogeneous Fluid

To obtain a scale for the Ekman-forced lateral flow in a homogeneous fluid, we solve for the currents of a progressive tidal wave in a linear, homogeneous, rotating channel in a manner similar to Kalkwijk and Booij (1986) and Geyer (1993). We assume that the field variables vary harmonically in time at the tidal frequency ($u, v, w, \zeta \sim e^{-i\sigma t}$), and that the dominant balance in the along-channel momentum equation is

$$u_t = -g\zeta_x + A_v u_{zz}. \tag{A1}$$

We impose that the barotropic pressure gradient is consistent with a progressive tidal wave ($\zeta_x \equiv i\sigma U_o/g$, where U_o is the amplitude of the tidal wave), and we assume that u vanishes at $z = -H$ and the stress vanishes at the surface, giving

$$u = \mathrm{Re}\left\{U_o\left[1 - \frac{\cosh(\kappa z)}{\cosh(\kappa H)}\right]e^{-i\sigma t}\right\}, \tag{A2}$$

where $\kappa^2 = -i\sigma/A_v$. In the cross-channel direction, we assume that the vertically averaged cross-channel current $\overline{v}$ is much smaller than the vertically averaged along-channel current $\overline{u}$, leading to the vertically averaged, cross-channel momentum balance:

$$f\overline{u} = -g\zeta_y - \frac{A_v}{H}v_z|_{z=-H}. \tag{A3}$$

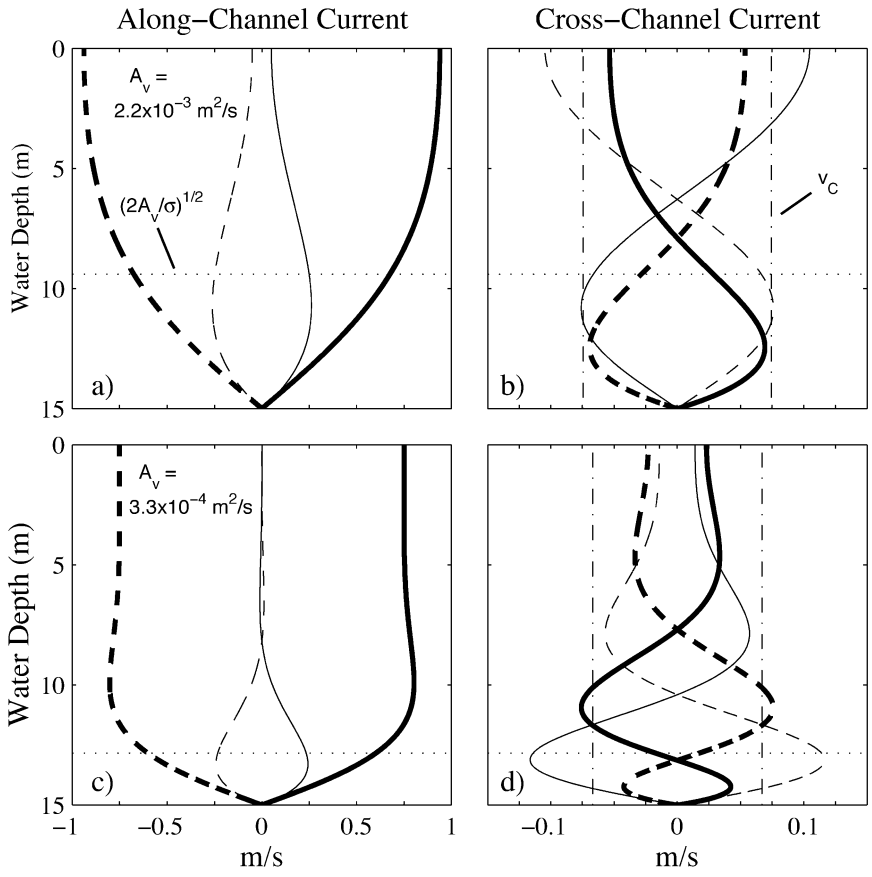

FIG. A1. Along-channel and cross-channel currents for a progressive tidal wave in a linear, homogeneous, rotating channel (see the appendix text) with a constant vertical eddy viscosity of (a), (b) 2.2×10^{-3} m^2 s^{-1} and (c), (d) 3.3×10^{-4} m^2 s^{-1}. The different curves correspond to different times within a tidal period. The horizontal dotted lines show the boundary layer thickness, and the vertical dot–dashed lines show the scaling for v_c in Eq. (2).

Subtracting this from the cross-channel momentum equation gives

$$v_t - f(u - \overline{u}) = A_v v_{zz} + \frac{A_v}{H} v_z|_{z=-H}. \quad \text{(A4)}$$

With the boundary conditions that v vanishes at the bottom and the stress vanishes at the surface, the solution for v is

$$v = \mathrm{Re}\left\{\frac{i}{2} U_o \frac{f}{\sigma}\left[\alpha \frac{\cosh(\kappa z)}{\cosh(\kappa H)} - \alpha \frac{\tanh(\kappa H)}{\kappa H} - \kappa z \frac{\sinh(\kappa z)}{\cosh(\kappa H)} - \frac{\tanh(\kappa H)}{\kappa H} + 1\right] e^{-i\sigma t}\right\},$$

where

$$\alpha = \frac{\kappa^2 H^2 \tanh(\kappa H)}{\kappa H - \tanh(\kappa H)} - 1. \quad \text{(A5)}$$

The structure of u and v is dependent on the thickness of the boundary layer, $|\kappa^{-1}|$, relative to the maximum depth of the fluid (Fig. A1). When the tidal boundary layer thickness is comparable to the channel depth (Figs. A1a and A1b), the cross-channel flow has a single cell structure, as depicted in Fig. 1c. For thin tidal boundary layers relative to the channel depth (Figs. A1c and A1d), cross-channel currents are concentrated in the bottom boundary layer and the vertical structure of the flow changes over a tidal cycle.

The strength of this Ekman-forced lateral flow does not have a simple scaling with respect to the boundary layer thickness ($\beta \equiv \sqrt{2A_v/\sigma}$). For $\beta/H \ll 1$, the vertically averaged amplitude of v increases with increasing boundary layer thickness for a given vertically averaged, along-channel tidal amplitude. It reaches a maximum value at $\beta/H \approx 0.2$ and then decreases with increasing boundary layer thickness. For the range of eddy viscosities considered in this study ($0.1 < \beta/H < 0.4$), the scale of the Ekman-forced lateral flow is roughly independent of β and is approximately

$$v_C \sim \frac{1}{8} \frac{f}{\sigma} U_o.$$

REFERENCES

Burchard, H., and H. Baumert, 1995: On the performance of a mixed-layer model based on the k–ϵ turbulence closure. *J. Geophys. Res.*, **100,** 8523–8540.

Chant, R. J., 2002: Secondary circulation in a region of flow curvature: Relationship with tidal forcing and river discharge. *J. Geophys. Res.*, **107,** 3131, doi:10.1029/2001JC001082.

——, and R. E. Wilson, 1997: Secondary circulation in a highly stratified estuary. *J. Geophys. Res.*, **102,** 23 207–23 216.

Chatwin, P. C., 1976: Some remarks on the maintenance of the salinity distribution in estuaries. *Estuarine Coastal Mar. Sci.*, **4,** 555–566.

Fischer, H. B., 1972: Mass transport mechanisms in partially stratified estuaries. *J. Fluid Mech.*, **53,** 671–687.

Friedrichs, C. T., and J. M. Hamrick, 1996: Effects of channel geometry on cross-sectional variations in along-channel velocity in partially stratified estuaries. *Buoyancy Effects on Coastal and Estuarine Dynamics*, D. G. Aubrey and C. T. Friedrichs, Eds., Amer. Geophys. Union, 283–300.

Garrett, C., P. MacCready, and P. Rhines, 1993: Boundary mixing and arrested Ekman layers: Rotating stratified flow near a sloping boundary. *Annu. Rev. Fluid Mech.*, **25,** 291–323.

Geyer, W. R., 1993: Three-dimensional tidal flow around headlands. *J. Geophys. Res.*, **98,** 955–966.

——, and H. M. Nepf, 1996: Tidal pumping of salt in a moderately stratified estuary. *Buoyancy Effects on Coastal and Estuarine Dynamics*, D. G. Aubrey and C. T. Friedrichs, Eds., Amer. Geophys. Union, 213–226.

——, R. P. Signell, and G. C. Kineke, 1998: Lateral trapping of sediment in a partially mixed estuary. *Physics of Estuaries and Coastal Seas*, J. Dronkers and M. Scheffers, Eds., Balkema, 115–126.

——, J. H. Trowbridge, and M. M. Bowen, 2000: The dynamics of a partially mixed estuary. *J. Phys. Oceanogr.*, **30,** 2035–2048.

Guymer, I., and J. R. West, 1992: Longitudinal dispersion coefficients in an estuary. *J. Hydraul. Eng.*, **118,** 718–734.

Haidvogel, D. B., H. Arango, K. Hedstrom, A. Beckmann, P. Malanotte-Rizzoli, and A. Shchepetkin, 2000: Model evaluation experiments in the North Atlantic Basin: Simulations in nonlinear terrain-following coordinates. *Dyn. Atmos. Oceans*, **32,** 239–281.

Hansen, D. V., and M. Rattray, 1965: Gravitational circulation in straits and estuaries. *J. Mar. Res.*, **23,** 104–122.

Ianniello, J. P., 1977: Tidally induced residual currents in estuaries of constant breadth and depth. *J. Mar. Res.*, **35,** 755–786.

——, 1979: Tidally induced residual currents in estuaries of variable breadth and depth. *J. Phys. Oceanogr.*, **9,** 962–974.

Johnson, G. C., and D. R. Ohlsen, 1994: Frictionally modified rotating hydraulic channel exchange and ocean outflows. *J. Phys. Oceanogr.*, **24,** 66–78.

Kalkwijk, J. P. T., and R. Booij, 1986: Adaptation of secondary flow in nearly-horizontal flow. *J. Hydraul. Eng.*, **24,** 19–37.

Kantha, L. H., and C. A. Clayson, 1994: An improved mixed layer model for geophysical applications. *J. Geophys. Res.*, **99,** 25 235–25 266.

Lacy, J. R., and S. G. Monismith, 2001: Secondary currents in a curved, stratified, estuarine channel. *J. Geophys. Res.*, **106,** 31 283–31 302.

Li, C., and J. O'Donnell, 1997: Tidally driven residual circulation in shallow estuaries with lateral depth variation. *J. Geophys. Res.*, **102,** 27 915–27 929.

Mellor, G. L., and T. Yamada, 1982: Development of a turbulence closure model for geophysical fluid problems. *Rev. Geophys. Space Phys.*, **20,** 851–875.

Nepf, H. M., and W. R. Geyer, 1996: Intratidal variations in stratification and mixing in the Hudson estuary. *J. Geophys. Res.*, **101,** 12 079–12 086.

Nunes, R. A., and J. H. Simpson, 1985: Axial convergence in a well-mixed estuary. *Estuarine Coastal Shelf Sci.*, **20,** 637–649.

Ott, M. W., and C. Garrett, 1998: Frictional estuarine flow in Juan de Fuca Strait, with implications for secondary circulation. *J. Geophys. Res.*, **103,** 15 657–15 666.

——, R. Dewey, and C. Garrett, 2002: Reynolds stresses and secondary circulation in a stratified rotating shear flow. *J. Phys. Oceanogr.*, **32,** 3249–3268.

Peters, H., and R. Bokhorst, 2001: Microstructure observations of turbulent mixing in a partially mixed estuary. Part II: Salt flux and stress. *J. Phys. Oceanogr.*, **31,** 1105–1119.

Scott, C. F., 1994: A numerical study of the interaction of tidal oscillations and non-linearities in an estuary. *Estuarine Coastal Shelf Sci.*, **39,** 477–496.

Seim, H. E., and M. C. Gregg, 1997: The importance of aspiration and channel curvature in producing strong vertical mixing over a sill. *J. Geophys. Res.*, **102,** 3451–3472.

Simpson, J. H., J. Brown, J. Matthew, and G. Allen, 1990: Tidal

straining, density currents, and stirring in the control of estuarine stratification. *Estuaries,* **13,** 125–132.
Smith, R., 1976: Longitudinal dispersion of a buoyant contaminant in a shallow channel. *J. Fluid Mech.,* **78,** 677–688.
——, 1980: Buoyancy effects upon longitudinal dispersion in wide well-mixed estuaries. *Proc. Roy. Soc. London,* **296A,** 467–496.
——, 1996: Combined effects of buoyancy and tides upon longitudinal dispersion. *Buoyancy Effects on Coastal and Estuarine Dynamics,* D. G. Aubrey and C. T. Friedrichs, Eds., Amer. Geophys. Union, 319–329.
Stacey, M. T., S. G. Monismith, and J. R. Burau, 1999: Observations of turbulence in a partially stratified estuary. *J. Phys. Oceanogr.,* **29,** 1950–1970.
——, J. R. Burau, and S. G. Monismith, 2001: Creation of residual flows in a partially stratified estuary. *J. Geophys. Res.,* **106,** 17 013–17 037.
Trowbridge, J. H., W. R. Geyer, M. M. Bowen, and A. J. Williams III, 1999: Near-bottom turbulence measurements in a partially mixed estuary: Turbulent energy balance, velocity structure, and along-channel momentum balance. *J. Phys. Oceanogr.,* **29,** 3056–3072.
Valle-Levinson, A., C. Li, K.-C. Wong, and K. M. M. Lwiza, 2000: Convergence of lateral flow along a coastal plain estuary. *J. Geophys. Res.,* **105,** 17 045–17 061.
Warner, J. C., C. R. Sherwood, H. G. Arango, and R. P. Signell, 2004: Performance of four turbulence closure models implemented using a generic length scale method. *Ocean Modell.,* in press.
Weatherly, G. L., and P. J. Martin, 1978: On the structure and dynamics of the oceanic bottom boundary layer. *J. Phys. Oceanogr.,* **8,** 557–570.
West, J. R., and J. S. Mangat, 1986: The determination and prediction of longitudinal dispersion coefficients in a narrow, shallow estuary. *Estuarine Coastal Shelf Sci.,* **22,** 161–181.
Wilcox, D. C., 1998: *Turbulence Modeling for CFD.* DCW Industries, Inc., 540 pp.
Wong, K.-C., 1994: On the nature of transverse variability in a coastal plain estuary. *J. Geophys. Res.,* **99,** 14 209–14 222.
Woodruff, J. D., W. R. Geyer, C. K. Sommerfield, and N. W. Driscoll, 2001: Seasonal variation of sediment deposition in the Hudson River estuary. *Mar. Geol.,* **179,** 105–119.
Wunsch, C., 1970: On oceanic boundary mixing. *Deep-Sea Res.,* **17,** 293–301.